Proceedings of the Combustion Institute 40 (2024) 105272

Contents lists available at ScienceDirect

Proceedings of the Combustion Institute

journal homepage: www.elsevier.com/locate/proci

Theoretical and kinetic analysis of anisole and cresol primary reactivity in pyrolysis and combustion

Luna Pratali Maffei *, Andrea Della Libera, Tiziano Faravelli, Carlo Cavallotti

Department of Chemistry, Materials and Chemical Engineering "G. Natta", Politecnico di Milano, P.zza Leonardo da Vinci 32, 20133 Milano, Italy

ARTICLE INFO

Keywords:
Lignocellulosic biomass
Anisole
Cresol
Variable reaction coordinate transition state theory

ABSTRACT

Anisole and ortho/para (o/p-) cresol are relevant oxygenated aromatic compounds representative of lignocellulosic biomass and potential octane boosters. Despite their significance, the existing literature fails to comprehensively interpret the fundamental aspects of their decomposition reactions. To bridge this gap, we employ high-level theoretical calculations to determine rate constants for key decomposition reactions of both C_7H_8O isomers and C_7H_7O resonance-stabilized radicals generated by bond-fission and abstraction reactions from C_7H_8O. The rate constant determined theoretically using Variable Reaction Coordinate Transition State Theory for the $C_6H_5O + CH_3$ is in quantitative agreement with experimental data. In contrast to what is currently implemented in kinetic models, CH_3 addition to the carbon sites of the aromatic ring is largely favored over anisole formation. Hence, large quantities of methyl-cyclohexadienones (MCHDs) form and stabilize at lower temperatures. Once formed, MCHDs can rapidly isomerize to cresols and eliminate CO. Cresols unimolecular decomposition was found to be slower than that of phenol, thus warning against rate rules adopted in kinetic models to estimate their reactivity. o/p-$OC_6H_4CH_3$ are the main radicals produced and they decompose to $C_5H_4CH_3 + CO$ or to $OC_6H_4CH_2 + H$. Notably, p-$OC_6H_4CH_3$ exhibits faster H loss due to the higher stability of the product. Conversely, the ortho radical undergoes rapid interconversion with o-$HOC_6H_4CH_2$ owing to the vicinal O and CH_3 groups.

Implementing the new theoretical calculations in the CRECK model, with appropriate automated lumping of o/p-MCHDs and o/p-C_7H_7O species, significantly impacts kinetic simulations of aromatics combustion, especially for anisole. Key findings include the substantial accumulation of MCHDs at lower temperatures and a larger fraction of ortho isomers, which suggests to reconsider lumping schemes for cresols adopted in the existing kinetic mechanisms. Finally, the underprediction of the high-temperature ignition of anisole, attributed to the insufficient consumption of cresols, advocates for a revision of their oxidation kinetics.

1. Introduction

In the ongoing energy transition, the valorization of lignocellulosic biomass is emerging as a viable route for the production of biofuels and chemicals via e.g., fast pyrolysis and catalytic depolymerization [1]. Among the oxygenated monoaromatic hydrocarbons (OAH) obtained, anisole ($C_6H_5OCH_3$) and cresols ($HOC_6H_4CH_3$) exhibit optimal characteristics as gasoline octane boosters due to their high volatility and heating value, while reducing soot emissions owing to their oxygen content. Anisole, in particular, featuring methoxy and phenoxy moieties, is chosen as a surrogate fuel to represent the decomposition and oxidation behavior of lignocellulosic biomass [2,3].

The low dissociation energy of the O–CH_3 bond (64.2 kcal/mol [4]) causes anisole to decompose at temperatures as low as 800 K [5]. This reaction also largely determines anisole ignition propensity [6]. Then, the reactivity of phenoxy (C_6H_5O) and methyl (CH_3) radicals guides the distribution of products under both pyrolysis and oxidation conditions [5,7]. Rather than with the oxygen, CH_3 preferentially recombines with the carbon sites of C_6H_5O, forming cresols and methylated C_5 species [2,3]. Cresols also form during the oxidation of benzaldehyde through the same reaction channels and of toluene [8], where methylphenyl radicals recombine with $O(^3P)$ and O_2 to form methyl phenoxy radicals ($OC_6H_4CH_3$).

Despite the relevance of the $C_6H_5O + CH_3$ reaction and the subsequent decomposition of cresols, these pathways are not accurately assessed in the literature. The rate constant of O–CH_3 bond-fission was

* Corresponding author.
E-mail address: luna.pratali@polimi.it (L. Pratali Maffei).

https://doi.org/10.1016/j.proci.2024.105272
Received 4 December 2023; Received in revised form 23 May 2024; Accepted 28 May 2024
Available online 1 July 2024

derived via plug flow (PF) or jet stirred (JS) reactor experiments of anisole thermolysis at 800–1600 K [9,10]. However, due to the fast reactivity between C_6H_5O and CH_3 radicals, data interpretation always required simple kinetic models incorporating at least the formation of cresols, phenoxy radical decomposition, and methyl self-recombination [10]. In particular, Lin and Lin [10] highlighted the sensitivity of CO profiles to the $C_6H_5O + CH_3 = HOC_6H_4CH_3$ reaction, with a rate constant estimated to be $\sim 1.7 \times 10^{-13}$–10^{-12} cm^3/s at $T = 1000$–1600 K and $p = 0.4$–0.9 atm. The only available experimental estimate for the total $C_6H_5O + CH_3$ recombination rate constant was obtained via pulsed laser photolysis of anisole by Tonokura et al. [11] at $T = 298$ K and $p = 0.026$ atm, obtaining a value of $6.2 \pm 2.6 \times 10^{-11}$ cm^3/s. This result seems incompatible with the much lower cresol formation rate proposed in [10].

As regards theoretical calculations, Pecullan et al. [12] estimated rate constants for $C_6H_5O + CH_3 => C_6H_5OCH_3$, $HOC_6H_4CH_3$, $C_5H_5CH_3$ (methyl cyclopentadiene) + CO via QRRK analysis based on thermodynamic considerations. The total association rate constant was approximated as $\sim 10^{-11}$–10^{-10} cm^3/s. More recently, Koirala [13] presented a more complete set of rate constants for the main decomposition reactions of anisole and o/p-cresol, as well as H-atom abstraction reactions from several C_7H_8O isomers. Potential energy surfaces (PESs) were determined at the CBS-QB3 level of theory and rate constants were computed with QRRK and made available at the high-pressure limit and at 1 atm. Contrary to [12], Koirala found lower values for the $C_6H_5O + CH_3$ association rate.

Due to the low level of theory of previous literature studies and the disagreement between and within theory and experiments, the available rate constants for C_7H_8O decomposition reactions have large uncertainties. This low accuracy is reflected in kinetic models for anisole pyrolysis and oxidation. O–CH_3 bond fission rate constant is often taken from the experimental value of Arends et al. [9] (e.g., in [2,14]). The total rate constant for $C_6H_5O + CH_3$ recombination at $T > 800$ K is ~ 1–3×10^{-11} cm^3/s in several kinetic models, while the product distribution varies. As for cresols, most kinetic models lump together ortho (o-) and para (p-) isomers, while their decomposition reactivity is included from Pecullan et al. (as in [2]) or from Koirala (as in [7]), or estimated by analogy with phenol [6,14]. Finally, all kinetic schemes approximate the decomposition of C_7H_7O radicals from that of similar compounds (i.e., C_6H_5O).

In light of the identified knowledge gaps in determining the reaction kinetics of anisole and cresol, this work presents state-of-the-art theoretical calculations and master equation (ME) simulations for the decomposition of anisole, o/p-cresol, and of the C_7H_7O resonance-stabilized radicals formed by bond-fission and abstraction reactions. The new rate constants are incorporated into the CRECK kinetic model to test the impact of the theoretical findings on global kinetic simulations of the combustion of aromatics. Finally, performance analysis quantifies the different fractions of o/p- isomers and highlights reaction pathways of interest for future investigations.

2. Methods

2.1. Theoretical calculations

The PESs of interest in this work were explored with EStokTP [15], which relies on Gaussian 09 [16], Molpro 2021 [17] and MRCC [18] for electronic structure calculations and MESS [19] for master equation simulations. Rate constants were determined with the ab initio (AI-) transition state theory (TST)-based ME method. Geometry optimization and frequency calculations for all stationary points were performed at the ωB97X-D/6–311+*G*(d,p) level of theory. Single point energies (SPE) were refined at the FNO—CCSD(T) level using the cc-pVQZ-F12 and cc-pVTZ-F12 basis sets [20]. Extrapolation to the complete basis set limit (CBS) was obtained as E(QZ) + 0.69377*[E(QZ)-E(TZ)], with final accuracy of the relative energies estimated within 1 kcal/mol. Based on our previous findings for the analogous PES for phenol decomposition [21], the energy barriers for the three decarbonylation channels to form $C_5H_5CH_3$ were refined at the CASPT2(12e,11o) level of theory, using both aug-cc-pVTZ and cc-pVTZ/cc-pVQZ basis sets extrapolated to CBS and an IPEA shift of 0.25. The active space (AS) employed is analogous to that described in [21].

The thermochemistry of all thermochemically stable C_7H_8O, C_7H_7O and C_7H_6O isomers was derived post-processing the theoretical calculations with AutoMech [22]. Formation enthalpies were calculated at 0 K through the CBH-2 scheme [23], which reproduces the ATcT anisole literature value within 0.01 kcal/mol [4]. For cresols as well as radicals with resonance stabilization of the aromatic ring, isodesmic reactions involving C_6H_5OH, $C_6H_5CH_3$, C_6H_6, C_6H_5O, and $C_6H_5CH_2$ species were preferred. Upon testing of different schemes, the uncertainty in our predicted formation enthalpies is estimated to be below 0.5 kcal/mol for molecules and within 1 kcal/mol for radicals. The resulting thermochemical properties, fitted with NASA polynomials, are attached in the supplementary material (SM-2).

Conventional and variational TST (c/vTST) were employed to compute rate constants of channels with well-defined barriers. In particular, cTST was adopted for H-transfer reactions, while vTST was adopted for all the other channels such as ring opening and beta-scission reactions (see attached MESS input file for details). Internal rotors were treated with the 1D hindered rotor model as described in [15,19]. Torsional potentials were computed at 20° interval scans of the dihedral angles. Finally, the Eckart model [24] was adopted to account for tunneling corrections.

Rate constants for the addition of methyl to C_6H_5O and of H to o-$OC_6H_4CH_3$ were determined using Variable Reaction Coordinate (VRC-) TST using VaReCoF [25,26]. The semi-automated protocol implemented in EStokTP accelerated the setup of the VRC-TST simulations. First, a high-level (HL) potential along the minimum energy path (MEP) connecting the radical fragments was determined for each resonant radical site of both $C_6H_5O + CH_3$ and o-$OC_6H_4CH_3 + H$. The MEPs for the recombination of H atoms with the two o-$OC_6H_4CH_3$ meta sites were assumed to be energetically equivalent. Structures along the MEP were determined at the UωB97X-D/6–311+*G*(d,p) level of theory for 2.0–4.0 Å fragments separations. HL energies were determined at the CASPT2/aug-cc-pVTZ level using a (8e,8o) AS, consisted of the (2e,2o) electrons and orbitals of the radical centers and of the (6e,6o) π and π* bonding and antibonding orbitals of the aromatic ring. HL calculations were used to construct a correction potential for both HL energy and geometry relaxation to enable faster but accurate lower-level VRC-TST simulations. In particular, most VRC-TST samplings were performed with a minimal (2e,2o) AS and the smaller cc-pVDZ basis set using frozen fragment geometries determined at the UωB97X-D/6–311+*G*(d,p) level of theory. Instead, sampling for the O–CH_3 bond-fission of anisole required a larger (8e,8o) AS due to the non-negligible contribution of the π aromatic orbitals at the short separations where the minimum flux is reached (~2.1–2.6 Å). In our experience (e.g., $C_3H_6 + O(^3P)$ [27] and unpublished work on $CH_3 + NO_2$, $C_6H_5O + O(^3P)$ reactions), the use of DFT geometries obtained with broken symmetry guesses provides very close agreement with full CASPT2 optimizations, i.e., about 0.2 kcal/mol differences for the MEP and < 20 % differences in the final rate constant.

The branching for the recombination between the multiple resonant radical sites of C_6H_5O and o-$OC_6H_4CH_3$ was described by placing two pivot points (one above and one below the plane of the aromatic ring) on each of the four reactive sites. These pivot points were used for VRC-TST samplings at fragment separations of 2.0–5.0 Å to construct multifaceted dividing surfaces for short-range fluxes. Instead, single pivot points placed at the center of mass of each fragment were adopted at distances of 5–10 Å to build spherical dividing surfaces for long-range fluxes. The two fluxes were then included in the ME integration to determine channel-specific rate constant using a two TS model. Reaction fluxes for H association with p-$OC_6H_4CH_3$ were reasonably assumed identical to

those for o-$OC_6H_4CH_3$ and were only corrected for symmetry. Finally, o/p-$HOC_6H_4CH_2 + H$ recombination fluxes, which are less relevant from a kinetic standpoint, were estimated with phase space theory by reproducing literature values for the analogous $C_6H_5CH_2 + H$ reaction [28].

Rate constants were evaluated at $T = 500$–2000 K and $p = 0.01$–100 atm solving the multi-well one-dimensional ME [19]. Collisional energy transfer in Ar bath gas was computed through the exponential down model. The average energy transferred in a deactivating collision was estimated as $<\Delta E> = 366(T/298)^{0.47}$ cm^{-1} as proposed by Jasper [29] for cyclic molecules with alcohol groups. Lennard-Jones parameters were approximated from the critical properties of anisole [30] as $\sigma = 6.1$ Å and $\varepsilon = 411$ K. All MESS input files are attached as SM-1.

2.2. Kinetic modeling

The impact of the new theoretical findings on the global combustion reactivity of OAHs was tested with kinetic simulations of the pyrolysis and oxidation of anisole, cresols, and also benzaldehyde and toluene, where the reactivity of cresols might be relevant. All kinetic simulations were performed with OpenSMOKE++ [31]. The latest version of the CRECK kinetic model (a newer version of [14]) was updated with the results of this work. Compared to [14], the starting model contains revised $C_5H_5CH_3$ chemistry from [32], and additional $C_5H_4CH_3$ reactivity estimated by analogy with C_5H_5. Both $C_5H_5CH_3$ and $C_5H_4CH_3$ are lumped pseudospecies [32]. The CRECK model also considers ortho and para cresol as one. To test the impact of the present findings, the reactions involving cresol and the available C_7H_7O and C_7H_6O species (i.e., $OC_6H_4CH_3$, $HOC_6H_4CH_2$, $OC_6H_4CH_2$) were de-lumped assuming equal reactivity for the ortho and para isomers, obtaining an equivalent model.

Theoretical rate constants from ME simulations were lumped using our automated ME-based lumping approach (MEL) [33]. Thermochemistry of lumped pseudospecies was set equal to the most abundant isomer at equilibrated conditions [33]. The validity of the lumping procedure was assessed by comparing the performances of the detailed and lumped versions of the updated model. Modified Arrhenius fits for both the detailed and lumped sets of rate constants and pseudospecies compositions derived from MEL are available in SM-3.

3. Results and discussion

3.1. Potential energy surfaces

Fig. 1 depicts the main reaction channels for the C_7H_8O (a) and C_7H_7O para (b) and ortho (c) PESs investigated in this work. PRn products formed by H loss on the C_7H_8O PES correspond to the radicals Wn that decompose on the C_7H_7O PESs, as highlighted on Fig. 1b,c in parentheses. Additional details on species nomenclature are provided in Section S0. The only channel included for anisole decomposition is the bond-fission, as the access to other isomers on the PES (e.g., W-o) requires the transfer of H or CH_3 from the methoxy group to the aromatic ring with large TS barriers of 88.5 and 79.2 kcal/mol, respectively, similarly to H transfer reactions in alkylated aromatics [34]. CH_3 can also recombine on the ortho and para carbon sites of C_6H_5O and thus access the cresol PES via W-o and W-p, respectively. Instead, preliminary investigations at the DFT level of the direct radical H-atom abstraction by CH_3 from C_6H_5O revealed an energy barrier of ~25 kcal/mol, making this channel uncompetitive with the recombination reactions. The wells W-o and W-p isomerize to other methyl-cyclohexadienones (MCHDs: W-o/p, W2-o/p, W3-o/p, W6-o, W3B-o of Fig. 1a). Then, keto-enol tautomerization from W-o and W2-o/p can form o/p-cresol, as also observed in the analogous phenol system [21]. Instead, H transfers from the methyl group to the aromatic ring have much larger energy barriers (i.e., ~90 kcal/mol, see [34]) and were therefore neglected. The unstable W3-o/p and W3B-o diradicals undergo ring-closure and finally eliminate CO to form 1- and 2-$C_5H_5CH_3$. The latter is the rate determining step (RDS) for CO formation. H transfer and CO elimination from cresols and MCHDs compete with H losses to form resonance-stabilized

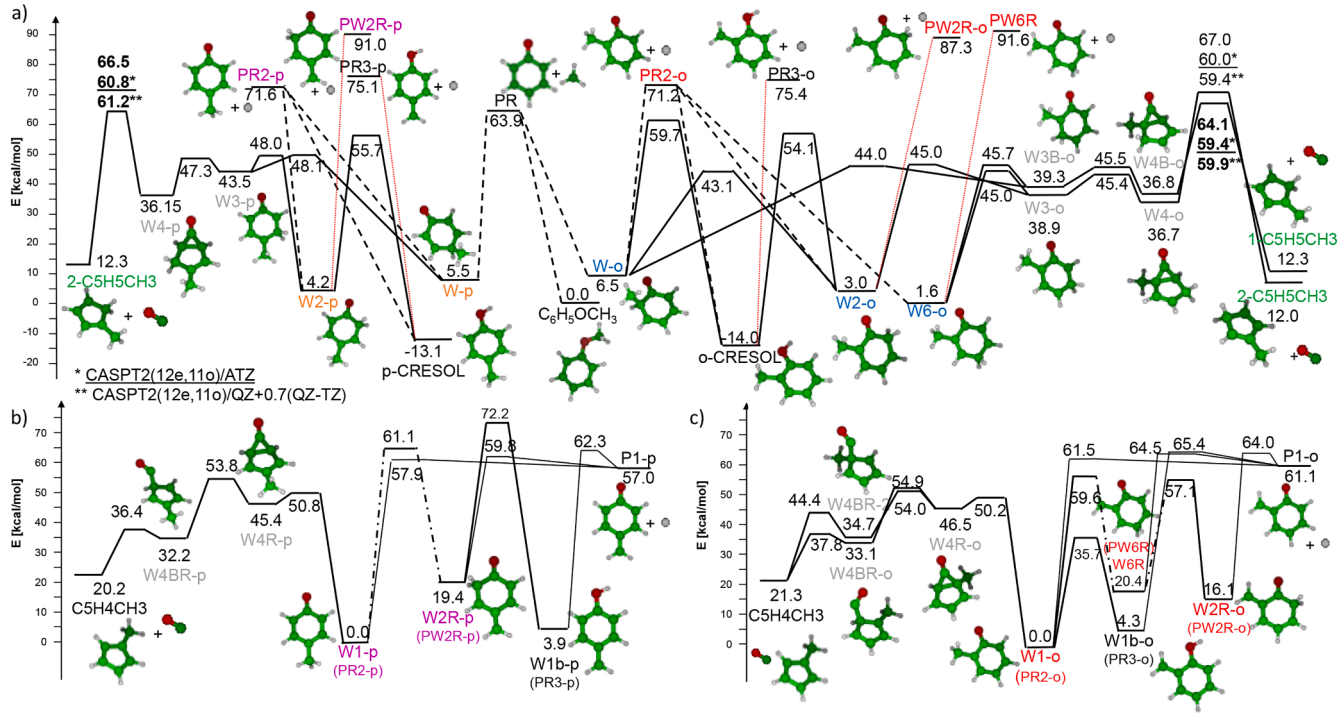

Fig. 1. Potential energy surfaces for the decomposition of C_7H_8O (a) and C_7H_7O para (b) and ortho (c) radicals. In (b) and (c), names in parentheses indicate the nomenclature of the corresponding species in (a). Energies are in kcal/mol and include Zero-Point corrections. Dash-dotted lines show that the PES was simplified for clarity (full PESs in Fig. S1). Name colors highlight different lumping treatment (Section 3.4): black = single species, grey = implicitly included, same color = same lumped group.

radicals, i.e., the phenoxy-like o/p-$OC_6H_4CH_3$ (PR2-o/p) and the benzyl-like o/p-$HOC_6H_4CH_2$ (PR3-o/p). At higher energies, H loss from the methyl groups of MCHDs can also lead to methylene-cyclohexadienonyl products (MeCHDyl: PW2R-o/p, PW6R). Overall, the decompositions of ortho and para cresol share similar reaction channels, however the former presents a larger number of MCHD isomers due to the lower symmetry, as well as faster conversion of W-o to the other MCHDs via H transfer to W2-o. The relative energies of analogous stationary points on the two portions of C_7H_8O PES are generally within 1 kcal/mol, except from W3 species and the associated TSs because of the stronger resonance of the W3-o/W3B-o rings. In comparison with the analogous mono-substituted phenol system [21], generally used as reference for cresol reactivity in kinetic models, energies of H-loss products PRn and the energy barrier for CO elimination are about 1–1.5 kcal/mol lower. This can be attributed to differences in the levels of theory adopted as well as to the presence of electron donating groups that stabilize the radicals, as observed for instance in ipso-substitution reactions on poly-substituted aromatics [35]. Additional details are discussed in Section S2.1.

Fig. 1b,c present the simplified PESs for the decomposition of p/o-C_7H_7O (full PESs in Fig. S1). Benzyl-like radical decomposition channels are expected to be energetically irrelevant and were not investigated. Both the ortho and para phenoxy-like radicals (W1-o/p) follow a radical decomposition pathway analogous to that of C_6H_5O => C_5H_5 + CO [21], with the RDS energy barriers being 0.7 and 0.9 kcal/mol above those computed in [21], consistent with the slightly higher stability of the substituted radicals. Due to its lower symmetry, W1-o can access two decomposition pathways: when the carbonyl and methyl moieties share the same carbon ring site (W4BR-2 of Fig. 1c), the higher steric hindrance increases the energy barriers by 0.9 and 6.6 kcal/mol for the three-membered ring opening and the CO loss, respectively. The vicinity of the C=O and C–CH_3 groups in W1-o also allows fast interconversion to W1b-o, contrary to the para system. Hence, the fate of the ortho radicals will be determined only after W1-o/W1b-o equilibration. Finally, both W1-o/p and W1b-o/p can undergo H transfer and then H loss to produce methylene-cyclohexadienones (MeCHDs: P1-o/p). These paths are unavailable to the unsubstituted phenoxy radical and may be relevant at high temperatures. P1-p is predicted to be 4.1 kcal/mol more stable than P1-o, as reflected directly on the energy barriers for the respective β-scission channels. Hence, H loss to $OC_6H_4CH_2$ will be favored in the para system with respect to the ortho one.

3.2. Rate constants of recombination channels

Rate constants for the C_6H_5O + CH_3 and o-$OC_6H_4CH_3$ + *H* recombination reactions were determined using VRC-TST as described in Section 2.1. Fig. 2a,b show the HL potentials determined along the MEPs. Interestingly, the MEPs for the formation of anisole and o-cresol are the least attractive, in contrast with the larger exothermicity of these channels with respect to the competing ones (see Fig. 1a). However, the radical center in C_6H_5O and o-$OC_6H_4CH_3$ is mostly located on the aromatic ring, while the oxygen atom is involved in a strong double bond. Additionally, the anisole MEP exhibits a minimum at O–CH_3 separations of ~3.5 Å. In fact, CH_3 establishes a non-bonding interaction with the aromatic ring and then re-orients to a parallel configuration at shorter distances, as shown in Fig. 2a.

Fig. 2c, d present the calculated total and channel-specific rate constants. The total C_6H_5O + CH_3 rate constant (Fig. 2c) is in quantitative agreement with the experimental measurement of Tonokura et al. [11]. It is noted that the total high-pressure rates of Fig 2c,d slightly differ from those at 1 atm even at low temperatures. This is not attributed to a fall-off behavior (present at $T > 1000$ K) but rather to the use of two different master equation models. It is noted that the long-range flux is computed with pivot points at the center of mass of the fragments, such that the recombination rate constant is not site-specific. Hence, it is necessary to choose how to partition the long-range flux among the

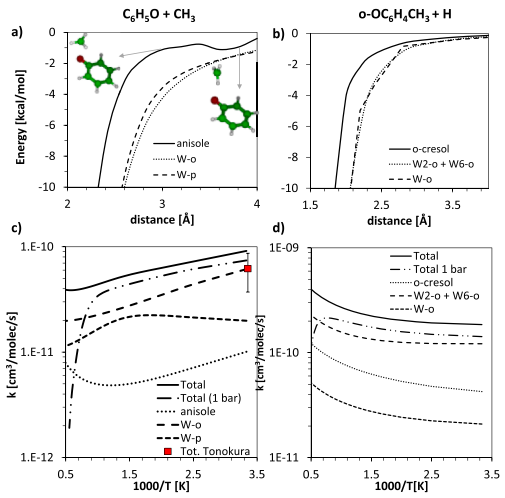

Fig. 2. CASPT2/aug-cc-pVTZ MEP potentials (ZPE excluded) for a) C_6H_5O + CH_3 and b) o-$OC_6H_4CH_3$ + *H* reactions, and corresponding total and channel-specific rate constants in c) and d), respectively, compared with the experimental data from Tonokura et al. [11]. Products nomenclature corresponds to that of Fig. 1.

different radical centers. This partitioning is relevant at low temperatures ($T < 600$ K), where the short- and long-range fluxes leading to W-o/p are comparable. High-pressure calculations (i.e., all lines in Fig. 2 except the "Total (1 bar)" rate) require separate master equation simulations for each site including both long and short-range fluxes. Hence, the long-range flux was split equally between the recombination on the oxygen center and on the aromatic ring. A more physically consistent model, used instead for pressure-dependent simulations, assumes that the long-range flux connects the reactants to the same van der Waals well, which is then connected to the final products. The identification of entrance van der Waals wells for the different recombination sites might impact the channel-specific rate constants only when the long range flux is rate controlling and was therefore deemed beyond the scope of the present work.

Overall, the channel-specific rate constants of Fig. 2c,d show that the slowest recombination channels lead to cresol and anisole, while addition on the aromatic ring is always favored. This behavior determines the subsequent reactivity and distribution of products, as discussed below.

3.3. Global kinetics and product distribution

This section summarizes the results of the global reactivity of the studied portions of the C_7H_8O and C_7H_7O PESs. Fig. 3a reports the branching fractions (BFs) of the main products of C_6H_5O + CH_3 at $p = 1$ atm. At low temperatures, anisole, W-o, and W-p stabilize thermochemically and accumulate. At higher temperatures, W-o and W-p convert to other MCHDs. The larger fraction of ortho MCHDs reflects both the faster methyl recombination on the ortho carbon site of C_6H_5O (Fig. 2c) and the fast conversion between W-o and W2-o (Section 3.1). At $T > 1500$ K, MCHDs isomerize to cresols or decompose prior to collisional stabilization, resulting in oscillating BFs. Because of the high rovibrational energy, well-skipping reactions produce $C_5H_5CH_3$ + CO, and H + C_7H_7O isomers, i.e., mostly $OC_6H_4CH_3$ with minor fractions of $HOC_6H_4CH_2$ (see Fig. S2). H loss prevails over CO elimination at $T >$ 1500–1600 K. Overall, at higher temperatures the main products are W2-o/p, o/p-cresol, o-$OC_6H_4CH_3$ + *H*, and $C_5H_5CH_3$ + CO.

While MCHD isomers are less stable than cresols, they can accumulate substantially at $T < 1600$ K. MCHDs isomerize fast, with rate constants of the order of 10^3–10^4 s^{-1} at $T = 1000$ K (Fig. S3, S4), and may thus form an equilibrated isomer pool. Dissociation to C_6H_5O + CH_3 is the favored decomposition channel (k(1000 K) = 10^1–10^3 s^{-1}), followed

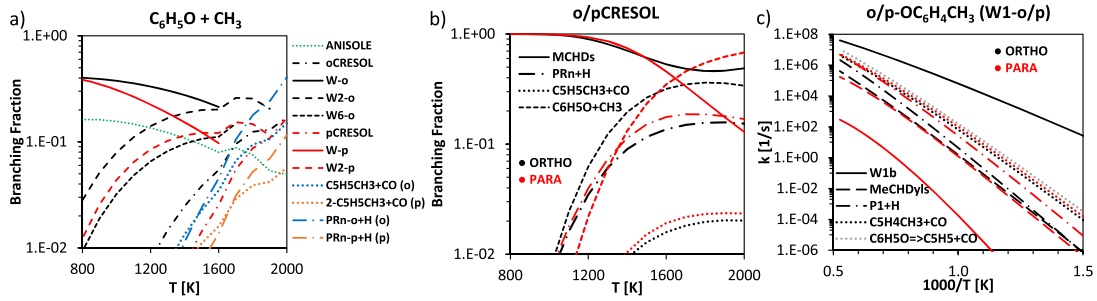

Fig. 3. Branching fractions for the products of a) $C_6H_5O + CH_3$ and b) ortho (o, black) and para (p, red) cresol decomposition; PRn are sums of H-loss products PRn-o/p. c) Rate constants for o/p-$OC_6H_4CH_3$ (W1-o/p) radical decomposition; MeCHDyls include isomerization to all the other wells except W1b-o/p. The rate constant of C_6H_5O decomposition from [21] is also plotted for comparison. Product names correspond to those of Fig. 1. All data refer to $p = 1$ atm.

by CO elimination (k(1000 K) = 1–10 s^{-1}), while H loss reactions are the slowest. It is noted that MCHDs are generally excluded from combustion models for OAHs as they are assumed to convert rapidly to cresols, similar to what commonly done for C_6H_6O isomers [21]. However, MCHDs may be formed at low temperatures such as in anisole combustion and therefore accumulate, as assessed in the kinetic simulations discussed in Section 3.4.

Fig. 3b shows branching fractions for the main products of o/p-cresol decomposition at 1 atm (detailed products in Fig. S5). The reactivity of the o/p- isomers is analogous and it proceeds mostly via isomerization to MCHDs at low temperatures, and dissociation to $C_6H_5O + CH_3$ and PRn + *H* at higher temperatures, with PRn indicating H loss products (see Fig. 1a). Direct CO elimination is a minor pathway, as opposed to the reactivity of MCHDs. Compared to p-cresol, o-cresol shows larger formation of $C_6H_5O + CH_3$ at intermediate temperatures and smaller production of H and CO, while isomerizations dominate at all temperatures. This behavior reflects both the higher stability of o-cresol related to the interaction between the side hydroxy and methyl groups and the faster dissociation to $C_6H_5O + CH_3$ via o-cresol = W2-*o* = *W*-o pathway. In terms of global reactivity, compared to phenol [21] the temperature dependence and relative importance of the H loss and CO elimination channels are similar. However, despite the lower energy barriers, the decomposition of cresols is slower (factors of 1.5–4.0 at T = 800–1200 K), reasonably because of the larger steric hindrance of the lateral methyl group, warning against currently adopted analogy rules. Additional details are discussed in Section S2.2.

Fig. 3c shows the rate constants of the decomposition channels of o/p-$OC_6H_4CH_3$ radicals (W1-o/p of Fig. 1; detailed rate constants in Fig. S6a,e), which are the main products formed by H loss from C_7H_8O. The most striking difference between the reactivity of W1-o and W1-p is the fast H transfer from W1-o to W1b-o. W1b-o product distribution is similar to that of W1-o (Fig. S6b). H transfer reactions to MeCHDyls (i.e., W2R-o/p, W6R of Fig. 1b,c) are minor in the full range of temperature, while CO elimination is the dominant decomposition reaction for both radicals. The rate constant for W1-*p* => $C_5H_4CH_3$ + CO agrees within a factor of 1.5 with our previous calculation for C_6H_5O => C_5H_5 + CO [21], while that for W1-*o* => $C_5H_4CH_3$ + CO is a factor of 2.3–3.4 slower than [21] due to both the higher energy barriers (see Fig. 1c) and the steric hindrance of the lateral methyl group. At higher temperatures, β-scission reactions to o/p-$OC_6H_4CH_2 + H$ (P1 + *H* in Fig. 3c) contribute up to 32 % and 47 % to the o/p-$OC_6H_4CH_3$ product distribution (excluding the W1-*o* = W1b-o channel), respectively; formation of p-$OC_6H_4CH_2 + H$ is faster than that of its ortho counterpart due to the larger stability of the product.

3.4. Lumping and kinetic modeling

Rate constants from ME simulations were lumped with MEL as described in Section 2.2. Colors of species names of Fig. 1 highlight lumped species, while thermochemically unstable isomers (in grey) were excluded. o/p-MCHDs were grouped together and show dominant fractions of W2-o/p. MeCHDyl isomers are produced in small amounts and were therefore grouped with the respective o/p-$OC_6H_4CH_3$ isomers (see Section S4). Consequently, only 2 new species were added to the model (i.e., o/p-MCHD named o/p-$OC_6H_5CH_3$, see SM-3). Overall, 76 new irreversible reactions were obtained thanks to lumping, while the full set of detailed rate constants included 13 species and 212 reactions. The main differences in the updated reactivity with respect to the reference CRECK model are that 1) anisole bond-fission is a factor of 1.5–2 faster at $p \geq 1$ atm and $T \leq 1500$ K, while it becomes slower at p ⟨ < 1 atm and T ⟩ 1100 K; and 2) $C_6H_5O + CH_3$ recombination on the aromatic ring sites is about 3 times faster and mostly produces MCHDs instead of cresols. Preliminary kinetic simulations revealed substantial accumulation of MCHDs, therefore bimolecular reactions involving MCHDs were included in the model, mostly by analogy with toluene (see Section S5).

The impact of kinetic model updates was most evident on kinetic simulations of literature anisole pyrolysis and combustion experiments. First, it is noted that anisole conversion is largely governed by the kinetics of the O–CH_3 bond-fission and therefore by the thermochemical properties of anisole. Compared to the values currently adopted in kinetic models [14,36], we predict lower formation enthalpies (by 1–2 kcal/mol in the 1000–2000 K range) mostly due to the lower heat capacity (by up to 2.3 cal/mol/K at 1000 K) and lower entropies (by 1–4 cal/mol/K). While our formation enthalpy matches within 0.1 kcal/mol the recommended value by ATcT at 298 K [4], the computed heat capacity underestimates the experimental values of Hales et al. [37] by ~1.5 cal/mol/K in the 400–500 K range, which are instead in better agreement with the values adopted in [14,36]. Overall, the computed Gibbs free energy increases by 1–6 kcal/mol in the 500–2000 K range (mostly due to the entropic contribution), which can shift the simulated anisole conversion profiles by 10–30 K, as reported more extensively in Section S3.2. Indeed, these discrepancies encourage additional experimental and theoretical investigations of anisole thermochemistry. Additionally, while there is better agreement in the literature on the thermochemical properties of the phenoxy radical, we believe that more accurate estimates might also be needed. The results here presented include the computed anisole bond-fission rate constant in its explicit forward and backward directions.

Fig. 4a shows profiles of some relevant species detected during anisole pyrolysis in PFR experiments [7]. The flux analysis of Fig. 5 guides the discussion on the reactivity. Anisole conversion in the new model increases at T ⟨ 1000 K, while it decreases at T ⟩ 1050 K and $p = 0.04$ atm, consistently with the updated rate constant of anisole bond-fission. The higher amount of C_6H_5O forms larger fractions of dibenzofuran ($C_{12}H_8O$) via self-association. About 75 % of C_6H_5O recombines with CH_3 to form MCHDs, with an o/p ratio of ~1.5. MCHDs either convert to cresols via H-transfer or to o/p-$OC_6H_4CH_3$ by H abstraction reactions, resulting in the early onset of $OC_6H_4CH_3$. o/p-$OC_6H_4CH_3$ eliminate CO and are the main source of $C_5H_4CH_3$. As anticipated in Section 3.3,

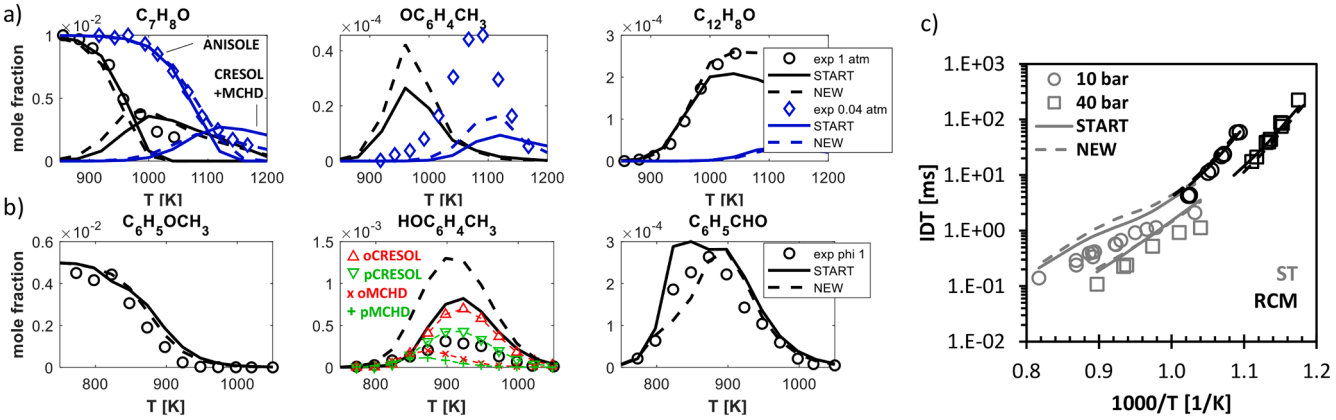

Fig. 4. Experimental and simulated mole fraction profiles of significant species in anisole a) pyrolysis in a PFR [7] and b) oxidation in a JSR [33]. c) Experimental and simulated ignition delay times at φ = 1 in the ST/RCM of [6].

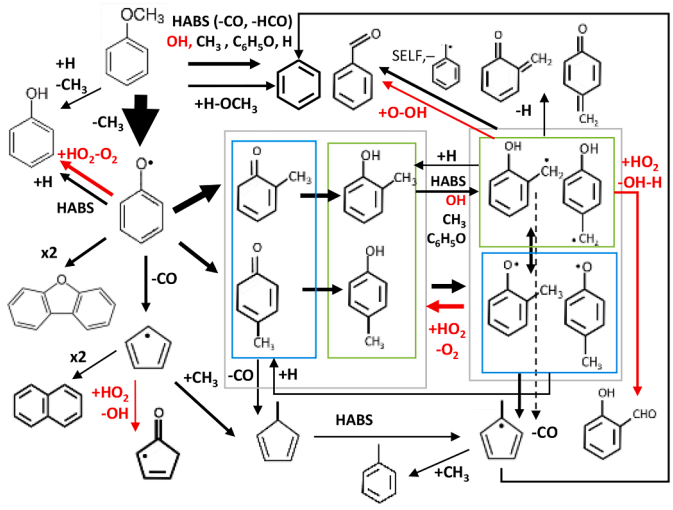

Fig. 5. Flux analysis for relevant pathways of anisole consumption (50 % conversion, $p = 1$ atm) in the reactors of Fig. 4a, b. Red paths are only active in oxidation conditions.

o-$OC_6H_4CH_3$ equilibrates with o-$HOC_6H_4CH_2$, thus the latter decarbonylates via well-skipping. Both o/p-$HOC_6H_4CH_2$ can be formed by H abstractions from cresols, and mainly recombine or lose H atoms.

Fig. 4b shows relevant species profiles for anisole oxidation (φ = 1) in a JSR [38]. Anisole conversion increases also in this case. The interesting change in shape at T ~825 K is due to the competition between the bond-fission and H abstractions by OH, that produce directly C_6H_5CHO. The former prevails in the updated model, as reflected by the strong decrease in C_6H_5CHO at $T < 900$ K. Instead, the faster C_6H_5O + CH_3 recombination to MCHDs and cresols leads to a strong overprediction of these species, which is in line with the slow cresol conversion obtained in JSRs for cresol oxidation (Fig. S19, S20). The mole fraction profiles of o/p-MCHD and o/p-cresol in Fig. 4b show that 1) MCHDs accumulate first and then isomerize to cresols; 2) the ortho isomers are more abundant, suggesting the possible need to differentiate the reactivity of o/p-cresol isomers in kinetic models. Similar observations result from the analysis of additional flow reactor experiments presented in Section S6.1. Overall, cresols are overpredicted, while simulated CO profiles are more aligned with experimental findings. The relevance of MCHDs emerges from the substantial impact of their reactivity even on the shape of the simulated species profiles (e.g., Figure S15). Finally, recombination reactions of C_7H_7O with other radicals (e.g., C_7H_7O, C_7H_7, CH_3) are key in determining the final product distribution, hence warranting more attention in future works.

Fig. 4c shows model predictions of anisole ignition delay times in ST and RCM experiments [6]. While the low-temperature acceleration is coherent with the JSR/PFR behavior, the reactivity slows down significantly at $T > 1000/1050$ K, $p = 10$ bar, similar to kinetic simulations of high-temperature premixed flame experiments (Figure S18). In fact, in the updated model anisole consumption by H abstractions to the reactive C_6H_5CHO decreases in favor of O–CH_3 bond-fission; then, C_6H_5O + CH_3 and subsequent reactions lead to large amounts of stable cresols and C_7H_7O radicals compared to the original model (four-fold and two-fold, respectively), thus slowing down the ignition. Overall, the present findings suggest the need to revise and further explore the oxidation reactivity of cresols and their radicals in kinetic mechanisms. A more detailed account of all kinetic simulations is reported in Section S6.

4. Conclusions

This work presents state-of-the-art theoretical calculations for the decomposition of anisole, o/p-cresol, and the associated C_7H_7O radicals. The C_7H_8O PES is accessed by C_6H_5O + CH_3 and $OC_6H_4CH_3$ + H reactions, which were studied with accurate VRC-TST calculations obtaining quantitative agreement with experiments. CH_3 recombines preferentially with the aromatic ring sites, leading to the low-temperature accumulation of large amounts of MCHDs, which can then isomerize to cresols. At higher temperatures, C_7H_8O largely decomposes back to C_6H_5O + CH_3, but can also form $C_5H_5CH_3$+ CO (especially MCHDs) or C_7H_7O + H (mostly cresols) as in the phenol system. However, cresol decomposition kinetics is slower than that of phenol, warning against analogies adopted in kinetic models. Finally, C_7H_7O radicals decompose to $C_5H_4CH_3$ + CO with similar reactivity to phenoxy.

The new rate constants were implemented in CRECK kinetic model and were found to substantially affect the global reactivity of anisole. The results of kinetic simulations highlight that 1) MCHDs accumulate significantly and therefore deserve more attention in kinetic schemes; 2) the fractions of ortho and para isomers are different and this should be reflected in lumped models; 3) thermochemical properties of anisole and of the phenoxy radical might need revision. Finally, bimolecular reactions involving cresol and their radicals should be further addressed to resolve model shortcomings such as the accumulation of cresols and the slow anisole ignition at high temperatures.

Novelty and significance statement

This work is novel as it presents the first high-level theoretical investigation of the main reaction channels active on the C_7H_8O potential energy surface for the unimolecular decomposition of anisole,

ortho- and para-cresol, as well as the subsequent unimolecular reactivity of the C_7H_7O radicals formed by H-loss reactions. VRC-TST treatment of bond-fission channels allowed quantitative agreement with experimental observations. The significance of the study was proved by 1) highlighting inaccuracies in rate constants currently adopted in kinetic models and 2) kinetic simulations of the combustion of anisole, cresol and other aromatics, showing large impact of the updated kinetics especially on the ignition propensity and on the product distribution of anisole pyrolysis and oxidation. Model performance analysis revealed the need to revise the cresol submodel. The present work will thus contribute to build accurate kinetic models for anisole and cresol, used as surrogate fuels of lignocellulosic biomass and biomass-derived biofuels.

Author contributions

- LPM: research design, PESs exploration, kinetic modeling, paper writing.
- ADL: VRC-TST calculations.
- TF: research design, paper writing.
- CC: research design, VRC-TST calculations, paper writing.
- All authors contributed to the write-up of the final version of the manuscript.

Declaration of competing interest

The authors declare that they have no known competing financial interests or personal relationships that could have appeared to influence the work reported in this paper.

Acknowledgements

This study was carried out within the NEST - Network 4 Energy Sustainable Transition (National Recovery and Resilience Plan (NRRP), Mission 4 Component 2 Investment 1.3; Concession Decree No. 1561 11/10/2022, Project code PE0000021) and reflects only the authors' views; neither the European Union nor Commission can be considered responsible for them.

Supplementary materials

Supplementary material associated with this article can be found, in the online version, at doi:10.1016/j.proci.2024.105272.

References

[1] F. Battin-Leclerc, N. Delort, I. Meziane, et al., Possible use as biofuels of monoaromatic oxygenates produced by lignin catalytic conversion: a review, Catal. Today. 408 (2023) 150–167.
[2] S.W. Wagnon, S. Thion, E.J.K. Nilsson, et al., Experimental and modeling studies of a biofuel surrogate compound: laminar burning velocities and jet-stirred reactor measurements of anisole, Combust. Flame. 189 (2018) 325–336.
[3] B. Chen, M. Hellmuth, S. Faller, et al., Exploring the combustion chemistry of anisole in laminar counterflow diffusion-flames under oxy-fuel conditions, Combust. Flame. (2021) 111929.
[4] B. Ruscic, D.H. Bross, Active Thermochemical Tables (ATcT) values based on ver. 1.122d of the Thermochemical Network Argonne National Laboratory, (2018).
[5] M. Nowakowska, O. Herbinet, A. Dufour, P.A. Glaude, Detailed kinetic study of anisole pyrolysis and oxidation to understand tar formation during biomass combustion and gasification, Combust. Flame. 161 (2014) 1474–1488.
[6] R.D. Büttgen, M. Tian, Y. Fenard, et al., An experimental, theoretical and kinetic modelling study on the reactivity of a lignin model compound anisole under engine-relevant conditions, Fuel 269 (2020) 117190.
[7] W. Yuan, T. Li, Y. Li, et al., Experimental and kinetic modeling investigation on anisole pyrolysis: implications on phenoxy and cyclopentadienyl chemistry, Combust. Flame. 201 (2019) 187–199.
[8] W. Yuan, Y. Li, P. Dagaut, J. Yang, F. Qi, Investigation on the pyrolysis and oxidation of toluene over a wide range conditions. I. Flow reactor pyrolysis and jet stirred reactor oxidation, Combust. Flame. 162 (2015) 3–21.
[9] I.W.C.E. Arends, R. Louw, P. Mulder, Kinetic study of the thermolysis of anisole in a hydrogen atmosphere, J. Phys. Chem. 97 (1993) 7914–7925.
[10] C.Y. Lin, M.C. Lin, Thermal decomposition of methyl phenyl ether in shock waves: the kinetics of phenoxy radical reactions, J. Phys. Chem. 90 (1986) 425–431.
[11] K. Tonokura, T. Ogura, M. Koshi, Near-UV absorption spectrum of the phenoxyl radical and kinetics of its reaction with CH_3, J. Phys. Chem. A. 108 (2004) 7801–7805.
[12] M. Pecullan, K. Brezinsky, I. Glassman, Pyrolysis and Oxidation of Anisole near 1000 K, J. Phys. Chem. A. 101 (1997) 3305–3316.
[13] Y. Koirala, Investigating the Kinetics of Anisole: a Simple Lignin Model Compound,. PhD Thesis, 2015.
[14] L. Pratali Maffei, M. Pelucchi, T. Faravelli, C. Cavallotti, Theoretical kinetics of HO_2+C_5H_5: a missing piece in cyclopentadienyl radical oxidation reactions, Proc. Combust. Inst. 39 (2023) 695–703.
[15] C. Cavallotti, M. Pelucchi, Y. Georgievskii, S.J. Klippenstein, EStokTP: electronic Structure to Temperature- and Pressure-Dependent Rate Constants—A Code for automatically predicting the thermal kinetics of reactions, J. Chem. Theory Comput. 15 (2019) 1122–1145.
[16] M. Frisch, G. Trucks, H.B. Schlegel, et al., Gaussian 09, revision D.01, (2013).
[17] H. Werner, P.J. Knowles, G. Knizia, F.R. Manby, M. Schütz, Molpro: a General-Purpose Quantum Chemistry Program Package, (2021).
[18] M. Kállay, P.R. Nagy, D. Mester, et al., The MRCC program system: accurate quantum chemistry from water to proteins, J. Chem. Phys. 152 (2020).
[19] Y. Georgievskii, J.A. Miller, M.P. Burke, S.J. Klippenstein, Reformulation and solution of the master equation for multiple-well chemical reactions, J. Phys. Chem. A. 117 (2013) 12146–12154.
[20] M. Kállay, R.A. Horváth, L. Gyevi-Nagy, P.R. Nagy, Basis set limit CCSD(T) energies for extended molecules via a reduced-cost explicitly correlated approach, J. Chem. Theory Comput. 19 (2023) 174–189.
[21] L. Pratali Maffei, M. Pelucchi, T. Faravelli, C. Cavallotti, Theoretical study of sensitive reactions in phenol decomposition, React. Chem. Eng. 5 (2020) 452–472.
[22] S.N. Elliott, K.B. Moore, A.V. Copan, et al., Automated theoretical chemical kinetics: predicting the kinetics for the initial stages of pyrolysis, Proc. Combust. Inst. 38 (2021) 375–384.
[23] R.O. Ramabhadran, K. Raghavachari, Theoretical thermochemistry for organic molecules: development of the generalized connectivity-based hierarchy, J. Chem. Theory Comput. 7 (2011) 2094–2103.
[24] C. Eckart, The penetration of a potential barrier by electrons, Phys. Rev. 35 (1930) 1303–1309.
[25] Y. Georgievskii, L.B. Harding, S.J. Klippenstein, VaReCoF : variable Reaction Coordinate Flux, https://tcg.cse.anl.gov/papr/codes/varecof.html, (2016).
[26] Y. Georgievskii, S.J. Klippenstein, Transition state theory for multichannel addition reactions: multifaceted dividing surfaces, J. Phys. Chem. A. 107 (2003) 9776–9781.
[27] A. Caracciolo, G. Vanuzzo, N. Balucani, et al., Combined experimental and theoretical studies of the $O(^3P)$ + 1-Butene reaction dynamics: primary products, branching fractions, and role of intersystem crossing, J. Phys. Chem. A. 123 (2019) 9934–9956.
[28] L.B. Harding, S.J. Klippenstein, Y. Georgievskii, On the combination reactions of hydrogen atoms with resonance-stabilized hydrocarbon radicals, J. Phys. Chem. A. 111 (2007) 3789–3801.
[29] A.W. Jasper, "Third-body" collision parameters for hydrocarbons, alcohols, and hydroperoxides and an effective internal rotor approach for estimating them, Int. J. Chem. Kinet. 52 (2020) 387–402.
[30] F.M. Mourits, F.H.A. Rummens, A critical evaluation of Lennard–Jones and Stockmayer potential parameters and of some correlation methods, Can. J. Chem. 55 (1977) 3007–3020.
[31] A. Cuoci, A. Frassoldati, T. Faravelli, E. Ranzi, OpenSMOKE++: an object-oriented framework for the numerical modeling of reactive systems with detailed kinetic mechanisms, Comput. Phys. Commun. 192 (2015) 237–264.
[32] B. Hanamirian, A. Della Libera, L. Pratali Maffei, C. Cavallotti, Investigation of Methylcyclopentadiene Reactivity: abstraction Reactions and Methylcyclopentadienyl Radical Unimolecular Decomposition, J. Phys. Chem. A. 127 (2023) 1314–1328.
[33] L. Pratali Maffei, M. Pelucchi, C. Cavallotti, A. Bertolino, T. Faravelli, Master equation lumping for multi-well potential energy surfaces: a bridge between ab initio based rate constant calculations and large kinetic mechanisms, Chem. Eng. J. 422 (2021) 129954.
[34] S.J. Klippenstein, L.B. Harding, Y. Georgievskii, On the formation and decomposition of C_7H_8, Proc. Combust. Inst. 31 (2007) 221–229.
[35] L. Pratali Maffei, T. Faravelli, C. Cavallotti, M. Pelucchi, Electronic structure-based rate rules for : h ipso addition-elimination reactions on mono-aromatic hydrocarbons with single and double OH/CH_3/OCH_3/CHO/C_2H_5 substituents: a systematic theoretical investigation, Phys. Chem. Chem. Phys. 22 (2020) 20368–20387.
[36] I. Meziane, N. Delort, O. Herbinet, R. Bounaceur, F. Battin-Leclerc, A comparative study of the oxidation of toluene and the three isomers of xylene, Combust. Flame. 257 (2023) 113046.
[37] J.L. Hales, E.B. Lees, D.J. Ruxton, Thermodynamic properties of organic oxygen compounds. Part 18.—Vapour heat capacities and heats of vaporization of ethyl ketone, ethyl propyl ketone, methyl isopropy1 ketone, and methyl phenyl ether, Trans. Faraday Soc. 63 (1967) 1876–1879.
[38] M. Nowakowska, O. Herbinet, A. Dufour, P.-A. Glaude, Detailed kinetic study of anisole pyrolysis and oxidation to understand tar formation during biomass combustion and gasification, Combust. Flame. 161 (2014) 1474–1488.